Environ. Sci. Technol. **2005**, *39,* 4808−4815

Spatial Distribution and Speciation of Lead around Corroding Bullets in a Shooting Range Soil Studied by Micro-X-ray Fluorescence and Absorption Spectroscopy

DELPHINE VANTELON,[†,‡] ANTONIO LANZIROTTI,[§] ANDREAS C. SCHEINOST,[†,∥] AND RUBEN KRETZSCHMAR*[,†]

Institute of Terrestrial Ecology, Swiss Federal Institute of Technology (ETH) Zurich, CH-8952 Schlieren, Switzerland, and The University of Chicago, Consortium for Advanced Radiation Sources, Chicago, Illinois

We investigated the spatial distribution and speciation of Pb in the weathering crust and soil surrounding corroding metallic Pb bullets in a shooting range soil. The soil had a neutral pH, loamy texture, and was highly contaminated with Pb, with total Pb concentrations in the surface soil up to 68 000 mg kg^{-1}. Undisturbed soil samples containing corroding bullets were collected and embedded in resin, and polished sections were prepared for micro-X-ray fluorescence (μ-XRF) elemental mapping and micro-X-ray absorption near edge structure (μ-XANES) spectroscopy. Bullet weathering crust material was separated from the metallic Pb cores and analyzed by powder X-ray diffraction analysis. Our results show a steep decrease in total Pb concentrations from the bullet weathering crust into the surrounding soil matrix. The weathering crust consisted of a mixture of litharge [α-PbO], hydrocerussite [$Pb_3(CO_3)_2(OH)_2$], and cerussite [$PbCO_3$], with litharge dominating near the metallic Pb core and cerussite dominating in the outer crust, which is in contact with the soil matrix. On the basis of these results and thermodynamic considerations, we propose that the transition of Pb species after oxidation of Pb(0) to Pb(II) follows the sequence litharge → hydrocerussite → cerussite. Consequently, the solubility of cerussite limits the activity of Pb^{2+} in the soil solution in contact with weathering bullets to $\leq 1.28 \times 10^{-6}$ at pH 7, assuming that the CO_2 partial pressure (P_{CO2}) in the soil is equal or larger than in the atmosphere ($P_{CO2} \geq 0.000\ 35$ atm).

Introduction

Contamination of soils with Pb is a widespread problem and can pose serious threats to human and ecosystem health (*1*). Pb is highly toxic to humans, grazing cattle, and wildlife. The greatest risk emanates from direct ingestion of bullets, contaminated soil or plants, and Pb-rich dust (*2*−*6*). Lead contamination of soils may stem from various sources, including mining and smelting of ores, deposition or recycling of spent batteries, waste incineration, and traffic (*7*, *8*). In many countries, the use of Pb-based ammunition is another significant source of Pb pollution. Annual Pb deposition by hunting and recreational shooting varies between 200 and 6000 t in The Netherlands, Denmark, Canada, and England and reaches 55 000 t in the United States (*9*−*12*). Switzerland has more than 2000 community shooting ranges used for mandatory shooting exercises of Swiss Army personnel and for recreational shooting. An estimated 90 million bullets are fired each year, resulting in an annual emission of 400−500 t of Pb (*12*). On many shooting ranges, the stop butt consists of a natural slope or of an artificial mound made of soil. Consequently, soils at and behind the stop butts are often highly contaminated, with maximum soil Pb concentrations ranging up to 150 000 mg kg^{-1} (*6*, *9*, *13*−*17*). For comparison, the average natural background concentration of Pb in soils is typically on the order of 10−30 mg kg^{-1} (*1*).

The environmental impact of soil contamination around shooting ranges has long been ignored, because the metallic Pb bullets were regarded as rather inert. However, once a bullet has penetrated the soil, the surface of the metallic Pb(0) core is slowly oxidized to Pb(II). The time required for complete oxidation and dissolution of Pb bullets in soils was estimated to range from 30 to 200 years, depending on soil chemical conditions (*9*, *18*). In the soil matrix, Pb^{2+} is strongly adsorbed by roots, soil organic matter, clays, calcite, or manganese and iron oxides (*1*, *6*, *8*). As long as corroding bullets are present in the soil, the secondary Pb phases in the weathering crusts control the Pb^{2+} activity in the soil solution surrounding the corroding bullets and are an important source of bioavailable Pb. It is therefore important to understand the mineralogical composition and spatial distribution of Pb species around corroding Pb bullets in soils. Several authors have investigated secondary Pb mineral species formed during metallic lead corrosion in soils by X-ray diffraction analysis. The most abundant secondary Pb phases were found to be hydrocerussite [$Pb_3(CO_3)_2(OH)_2$] and cerussite [$PbCO_3$] (*9*, *15*, *19*−*24*). In addition, massicot [β-PbO] has been reported to occur in weathering shotgun bullets (*15*, *21*, *22*) and litharge [α-PbO] in antique artifacts and weathered lead pipes (*23*, *24*). Small amounts of plattnerite [PbO_2], anglesite [$PbSO_4$], or hydroxypyromorphite [$Pb_{10}(PO_4)_6(OH)_2$] may also occur, depending on the soil chemical conditions. However, powder X-ray diffraction analysis may not detect amorphous or microcrystalline Pb phases and yields no direct information on the spatial distribution of Pb species. Using electron microprobe analysis (EMPA), Lin (*15*) observed weathering crusts around bullets exhibiting concentric rims with decreasing Pb concentration from the bullet core to the outer part of the crust. However, this technique does not allow a direct and spatially resolved investigation of Pb species. In the present study, we therefore apply a combination of micro-X-ray fluorescence (μ-XRF) and micro-X-ray absorption near-edge structure (μ-XANES) spectroscopy to investigate the spatial distribution and the speciation of Pb around corroding Pb bullets in shooting range soil.

Materials and Methods

Soil Samples. Soil samples were collected at a communal 300-m shooting range at Oberuzwil (47°25′51″ N, 9°7′12″ E) in the canton of St. Gallen, Switzerland. The shooting range

* Corresponding author phone: +41 44 6336003; fax: +41 44 6331118; e-mail: kretzschmar@env.ethz.ch.
† ETH Zurich.
‡ Present address: Paul Scherrer Institut, Swiss Light Source, CH-5232 Villigen. E-mail: delphine.vantelon@psi.ch.
§ The University of Chicago.
∥ Present address: The Rossendorf Beamline, European Synchrotron Radiation Facility, Grenoble, France. E-mail: scheinost@esrf.fr.

10.1021/es0482740 CCC: $30.25

Published on Web 05/21/2005

has been in operation for about 90 years. The shooting practice at the site consists primarily of rifle training with two calibers of bullets, 6.5 mm (GP11) and 7.5 mm (GW Pat 90). These bullets consist of a metallic core of Pb hardened with 2−4% Sb, encased in a cupronickel steel jacket. The stop butt is located within a natural slope. The immediate impact area is covered with a thin layer (1−2 cm) of sawdust to prevent bullet scattering. The surrounding area is vegetated by grass.

To characterize the magnitude and distribution of Pb pollution in the most heavily polluted area, we collected soil samples along a transect reaching from the target line across the stop butt area to 23 m behind the targets. To allow a more detailed sampling and the collection of undisturbed soil cores, a soil pit was opened 9 m behind the target, in the area with maximum bullet impact. The soil profile exhibited no distinct soil horizons, except a higher density of roots in the top 15 cm. No hydromorphic soil properties were observed, which indicates that the soil was well aerated during most parts of the year. Corroding bullets were observed in soil depths up to 90 cm. While these bullets most likely penetrated into the soil due to their impact energy, additional mixing of soil and bullets during the periodic renewal of the stop butt cannot be excluded. However, the exact history of reconstruction of the stop butt is unknown.

From the opened profile, in addition to collecting bullets and disturbed soil for bulk chemical and mineralogical analyses, we collected undisturbed soil samples, at depths of 25 cm (sample A) and 55 cm (sample B), for the microspectroscopic investigation. The samples were collected in custom-made $8 \times 6 \times 5$ cm^3 aluminum boxes, dried at 40 °C, and embedded in resin (LR White, SPI Supplies, West Chester, PA) at 60 °C under vacuum during 24 h. Each embedded soil sample, A and B, was cut into 50 sections, 250 μm thick, by use of a diamond saw; the sections were then polished with grit 500−5000 sandpaper (Accutom-50 and Labopol-5, Struers, Birmensdorf, Switzerland). Based on visual inspection of all sections, one representative section per box was selected for synchrotron μ-XRF and μ-XANES analysis.

Soil Analysis. Soil pH was measured with a combination pH electrode (Metrohm, Herisau, Switzerland) after 10 g of dry soil was equilibrated with with 25 mL of 0.01 M $CaCl_2$ solution for 30 min (*25*). Exchangeable cations were determined by extracting 2 g of soil with 20 mL of 1 M NH_4NO_3 solution for 24 h on a rotary shaker (*26*). The suspensions were then centrifuged for 15 min at 1500 g and the supernatant solutions were analyzed for Mg, Ca, Na, and K by atomic absorption spectrometry (Spectra 220FS, Varian, Palo Alto, CA). Selective sequential extractions (SSE) of the soil were performed following the seven-step procedure developed by Zeien and Brümmer (*26*). For total elemental analysis, the soils were ground to <60 μm in a vibratory disk mill (Retsch, Haan, Germany). Total C and N contents were measured on a CHNS analyzer (CHNS-932, Leco, St. Joseph, MI). Organic matter was extracted adding 1 g of soil in 15 mL of H_2O_2 at 50 °C during 24 h. Total concentrations of elements (Na to U) were determined by X-ray fluorescence spectrometry. Pellets (4 cm diameter) were pressed after 4 g of soil was thoroughly mixed with a binding component (C-Wachs, Hoechst) at a fixed soil/wax ratio of 40/9 and then analyzed on an energy-dispersive XRF spectrometer (X-Lab 2000, Spectro, Kleve, Germany). By using polarized X-ray radiation, a series of five secondary targets, and an ab initio method to improve the deconvolution of spectra, a lower detection limit of 0.5 mg kg^{-1} could be achieved for most elements. Accuracy of the XRF analysis was routinely verified by use of a certified standard sample (D133, MCACAL).

Analysis of Bullet Weathering Crust. The bullets collected in the soil pit excavated at 9 m behind the targets were physically deformed and strongly corroded, as indicated by a crust of brown and gray material. To analyze the corrosion products in this crust, six bullets were placed in a beaker, submerged in deionized water, and ultrasonicated at 300 W until no further crust material was removed. The resulting suspension with the crust material was then centrifuged and the sediment was air-dried and ground with an agate mortar. The material was then analyzed by powder X-ray diffraction (Scintag XRD-2000, Cupertino, CA) analysis with Cu Kα radiation (wavelength 1.5405 Å). The powder mounts were scanned over a Bragg angle range 2−70° 2θ with a step size of 0.02° 2θ and a scan rate of 2 s/step. Diffraction peaks were assigned by use of the Scintag DMSNT program (ICDD database, JCPDS card numbers 41-0677, 47-1734, 05-0490, 05-0561, and 05-0570). Total concentrations of elements were determined by XRF with the same protocol as for soil samples.

Elemental Mapping and μ-XANES. Elemental mapping in the energy range 2−20 keV was performed on a bench-scale μ-XRF instrument (μ-Eagle II, Röntgenanalytik GmbH, Taunusstein, Germany) equipped with a Rh X-ray tube (emission line ~20 000 eV) and a Si(Li) detector. The beam was focused by a polycapillary lens to a spot size of about 30 μm in diameter. Areas of 2.5×2 mm^2 were scanned with 20 μm step size and 5 s dwell time.

Pb L_{III} edge μ-XANES measurements were performed on beamline X-26A, at the National Synchrotron Light Source (NSLS), Brookhaven National Laboratory, Upton, NY. The incoming beam was focused to a spot size of 15 μm diameter by use of two 100 mm long, dynamically bent silica mirrors arranged in Kirkpatrick−Baez (KB) geometry (*27*). The soil sections were placed on a stage at an angle of 45° relative to the incident beam and could be observed with a CCD microscope. The Si(111) monochromator energy was calibrated relative to the L_{III} edge of metallic lead (13035 eV). For μ-XANES, six scans were collected in fluorescence mode with a lithium drifted silicon detector [Canberra SL30165 Si(Li)] at room temperature. Energy resolution was 1.8 eV around the Pb K edge. Synchrotron μ-XRF spectra were collected with 300 s dwell time and with 13.1 keV incident beam energy. Peak assignments and area calculations were performed with an IDL MCA routine developed at the beamline.

The XANES spectra were corrected for self-absorption by use of the FLUO code (version 002, May 1999) developed by Haskel (http://www.aps.anl.gov/xfd/people/haskel/fluo.html). They were normalized by use of a linear function for the pre-edge and a second-degree polynomial function for the postedge region. For statistical analysis, the spectra were smoothed by Fourier filtering. They were analyzed by linear combination fits with WinXAS 2.3 (*28*). The fits were performed across the edge from 13 010 to 13 110 eV. The energy was allowed to float during the fit within ±1 eV. Reference spectra were taken from the SSRL XAFS spectra library (http://www-ssrl.slac.stanford.edu/mes/spectra/compounds/pb/index.html).

Results and Discussion

Soil Contamination. Table 1 gives the total concentrations of Pb, Sb, Zn, Cu, and Ni of the soil samples collected along the lateral transect behind the target area. In the surface soil (0−5 cm depth), concentrations increase with increasing distance from the targets until the area of maximum bullet impact at around 9 m and then decrease again with distance. The maximum total Pb concentration is 68 g kg^{-1}. At 23 m behind the targets, the surface soil was still strongly contaminated with Pb. Similar trends along the transect were observed for Sb, Ni, Cu, and Zn, although the concentrations were lower owing to their lower concentrations in bullets (*12*). The concentration of Pb generally decreased with soil depth, although at 50 cm depth it was still above the average natural background concentration in soils. Extremely high

TABLE 1. Soil pH and Total Metal Concentrations[a]

distance from targets (m)	soil depth (cm)	soil pH (in 0.01 M $CaCl_2$)	metal concn (mg kg^{-1})				
			Ni	Cu	Zn	Sb	Pb
2	0−5	7.0	195	895	585	1100	23 620
2	5−15	7.1	180	835	645	605	14 330
2	15−25	7.1	100	300	360	315	5615
2	25−35	7.6	125	340	140	320	6435
2	35−45	7.6	150	750	350	365	10 860
2	45−55	7.4	80	285	70	150	5020
9	0−5	6.5	465	2250	570	3020	67 860
9	5−15	7.0	205	1055	900	755	16 090
9	15−25	7.1	280	1260	1025	905	19 100
9	25−35	7.3	155	690	1020	445	9950
9	35−45	7.3	65	210	1090	145	2250
9	45−65	7.6	100	250	115	230	4400
9	65−90	7.7	160	525	200	630	14 450
11	0−5	6.8	185	730	755	585	14 550
11	5−15	7.2	175	620	445	560	12 910
11	15−25	7.0	120	345	190	365	7540
11	25−45	6.5	45	25	70	60	235
11	45−65	7.2	60	30	80	35	390
11	65−90	7.9	40	25	55	10	165
13	0−5	6.8	145	375	160	590	13 440
13	5−15	6.7	70	70	80	115	2230
13	15−25	6.9	50	25	70	45	115
13	25−35	7.0	65	30	80	25	250
13	35−45	7.2	45	25	60	10	145
15	0−5	6.2	90	175	120	160	4405
15	5−15	7.2	90	135	105	100	2960
15	15−25	6.9	50	45	65	50	705
23	0−5	6.9	45	55	85	25	1045
23	5−15	5.0	50	120	80	35	1090
23	15−25	5.5	40	20	60	5	110

[a] Determined by XRF analysis as a function of soil depth along a transect ranging from 2 to 23 m behind the targets.

subsoil concentrations (>5000 mg kg^{-1}) of Pb were found at 2 and 9 m behind the targets (Table 1). Bullet fragments in the subsoils indicate that these elevated concentrations are related either to bullet penetration into the soil or to soil mixing by the periodic reconstruction and erosion of the stop butt.

Mineralogy of Soil and Corroding Bullets. The soil samples collected along the transect have slightly acidic to slightly alkaline pH values (Table 1) and clayey to loamy texture. A powder XRD analysis of the soil at 9 m behind the target revealed the following mineral composition: quartz (42%), muscovite (10%), dolomite (16%), calcite (14%), plagioclase (6%), microcline (5%), chlorite (5%), and hornblende (2%). The effective cation exchange capacity (ECEC) of the soil was 380 $mmol_c$ kg^{-1}, and Ca was the dominant exchangeable cation. The soil organic matter content ranged from 95 g kg^{-1} at 25 cm depth to 35 g kg^{-1} at 55 cm depth.

Figure 1 shows a powder XRD pattern of the weathering crust separated from corroding bullets collected at 9 m behind the targets. The mineral composition is cerussite (56%), quartz (23%), and hydrocerussite (12%), with smaller amounts of calcite (7%) and plagioclase (2%). Quartz, calcite, and plagioclase are minerals derived from the parent rock, while cerussite [$PbCO_3$] and hydrocerussite [$Pb_3(CO_3)_2(OH)_2$] are secondary Pb mineral phases formed during weathering of the Pb bullets (*9*, *15*, *19*).

Previous reports indicate that hydrocerussite is the most prevalent secondary Pb mineral phase (up to 80%) of bullet weathering in different soils with pH values ranging from 3 to 8 (*9*, *15*, *19*−*21*). In contrast to these previous studies, we found that cerussite was the predominant Pb mineral in the weathering crust. This difference may be due to a high CO_2 partial pressure in the Oberuzwil soil. Cerussite and hydrocerussite have similar solubilities, but elevated CO_2 partial pressures relative to the atmosphere favor the formation of cerussite over hydrocerussite (*23*, *29*). Traces of additional Pb mineral phases, such as massicot (β-PbO), plattnerite (α-PbO_2), hydroxypyromorphite [$Pb_{10}(PO_4)_6(OH)_2$], and anglesite [$Pb(SO_4)$], have been reported previously in different shooting range soils (*9*, *15*, *19*−*22*). In our samples, no additional Pb phase could be identified by XRD analysis except for traces of lead oxide (PbO). However, the signal of PbO was too weak to allow a nonambiguous assignment to either massicot (β-PbO) or litharge (α-PbO).

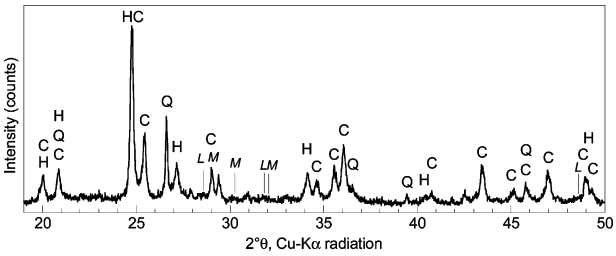

FIGURE 1. Bulk XRD pattern of the bullet crust material. H = hydrocerussite, C = cerussite, Q = quartz, L = litharge, M = massicot.

Selective Sequential Extraction. Table 2 presents the results of a selective sequential extraction applied to bulk soil samples collected in the vicinity of samples A and B. Only 0.5−1.3% of the total Pb was exctractable with a 1 M NH_4NO_3 solution (SSE 1), suggesting that only a very small percentage of the total Pb was bound by nonspecific cation exchange. The largest fraction of the total Pb (55−75%) was extractable with ammonium acetate at pH 6 (SSE 2). This extraction step is assumed to dissolve Pb associated with carbonates and also weakly complexed or chemisorbed Pb. This is in agreement with the high concentration of lead carbonate phases, cerussite and hydrocerussite, detected in the corrosion crust by XRD (Figure 1). The remaining Pb was extracted mainly with extraction steps SSE 3 and SSE 4, indicating Pb bound to manganese oxides and organic matter, respectively. A small fraction of the total Pb was in the residual phase extracted by total digestion (SSE 7). This residual fraction may include some metallic Pb(0).

Elemental mapping. Typical examples for the microscale elemental distribution around corroding Pb bullet cores are shown in Figures 2 and 3. On the optical microscope images of sample A (Figure 2a; 25 cm depth) and sample B (Figure 3a; 55 cm depth), the spots selected for μ-XANES analysis are marked. The metallic Pb bullet cores appear as light gray areas, labeled BC (spots 1A and 1B). The bullet core is surrounded by a dark gray weathering crust with a thickness of approximately 100 μm (spots 2A and 2B). In some areas, this gray material is covered with a second layer of light gray to white material (spots 3A and 3B), which is surrounded by the soil matrix (spots 4A and 4B). In Figure 3a, one can also see fragments of the dark gray material surrounded by white material, which appear to be similar to the weathering crust around the bullet core. Bullet steel jackets are not visible in these sections. Presumably, they have been separated from the core by the bullet impact into the soil.

Typical synchrotron μ-XRF spectra of the bullet core (Figure 4, spot 1A) are dominated by the two strongest X-ray emission lines (Pb $L\alpha_1$ at 10.552 keV and Pb $L\beta_1$ at 12.614 keV, Figure 4c). Weak Pb $M\alpha_1$ and $L\lambda$ lines are visible at 2.345 and 9.185 keV, respectively (Figure 4a,c). The strong decrease in Pb concentration from spot 1A (bullet core) to spot 4A (soil matrix at 250 μm distance from weathering crust) is evidenced by the strong decrease in the Pb fluorescence peaks. This trend is confirmed by the elemental mapping

TABLE 2. Results of Sequential Selective Extractions of Disturbed Soil Samples[a]

extraction step[b]	extracted Pb (% of total)[c] sample A	sample B	extracting solution (conditions)[b]	interpretation of Pb species[b]
SSE 1	1.3	0.6	1 M NH_4NO_3 (20 °C, 24 h)	exchangeable
SSE 2	74.2	54.3	1 M NH_4OAc, pH 6 (20 °C, 24 h)	bound to carbonates, weakly complexed
SSE 3	16.7	23.9	0.1 M NH_3OHCl + 1 M NH_4OAc, pH 6 (20 °C, 0.5 h)	bound to Mn (hydr)oxides
SSE 4	3.5	13.6	0.025 M NH_4EDTA, pH 4.6 (20 °C, 1.5 h)	bound to organic matter
SSE 5	0.8	1.3	0.2 M ammonium oxalate, pH 3.25 (20 °C, 4 h)	bound to Fe (hydr)oxides of low crystallinity
SSE 6	0.7	0.8	0.1 M ascorbic acid + 0.2 M ammonium oxalate, pH 3.25 (97 °C, 0.5 h)	bound to crystalline Fe (hydr)oxides
SSE 7	2.8	5.5	total digestion in concentrated HNO_3, HCl, HF (microwave)	bound in residual fraction

[a] Collected in the vicinity of sample A (25 cm depth) and sample B (55 cm depth). [b] According to Zeien and Brümmer (*26*). [c] Average of two replicates, total calculated as sum of all fractions.

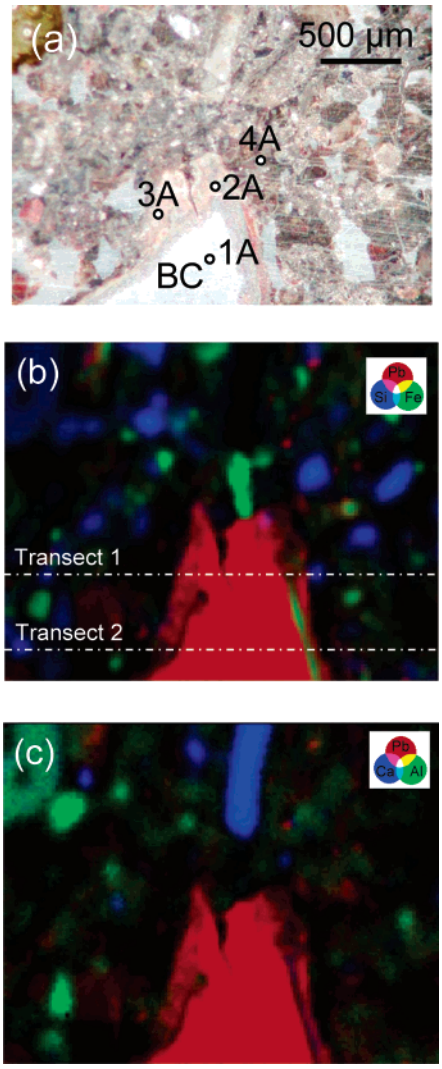

FIGURE 2. Photomicrographs of bullet area in sample A (a) (BC = bullet core) and X-ray fluorescence elemental maps: (b) Pb in red, Fe in green, Si in blue; (c) Pb in red, Al in green, Ca in blue. Maps were collected on a bench-scale μ-XRF instrument with a spot size of 30 μm. The step size is 20 μm and dwell time is 5 s. The map size is 2.5 × 2.0 mm^2.

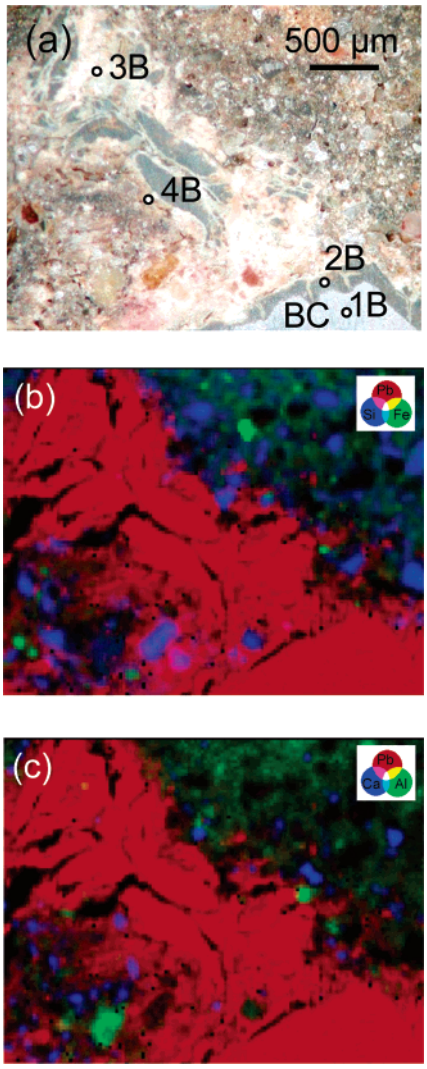

FIGURE 3. Photomicrographs of bullet area in sample B (a) (BC = bullet core) and X-ray elemental maps (b) Pb in red, Fe in green, Si in blue; (c) Pb in red, Al in green, Ca in blue. Maps were collected on a bench-scale μ-XRF instrument with a spot size of 30 μm. The step size is 20 μm and dwell time is 5 s. The map size is 2.5 × 2.0 mm^2.

(Figure 2b) and a transect concentration profile (Figure 5), which shows high Pb concentrations in the bullet core and the weathering crust and a sharp decrease in Pb counts in the surrounding soil (2 orders of magnitude within 200−300 μm). This sharp decrease is in agreement with Pb concentrations calculated from energy-dispersive XRF spectra collected for bulk soil (~15 000 mg kg^{-1} Pb) and crust (~180 000 mg kg^{-1} Pb) material. Despite the large number of corroded bullet fragments in sample B (Figure 3a), the sharp decrease in Pb concentration within a few hundred

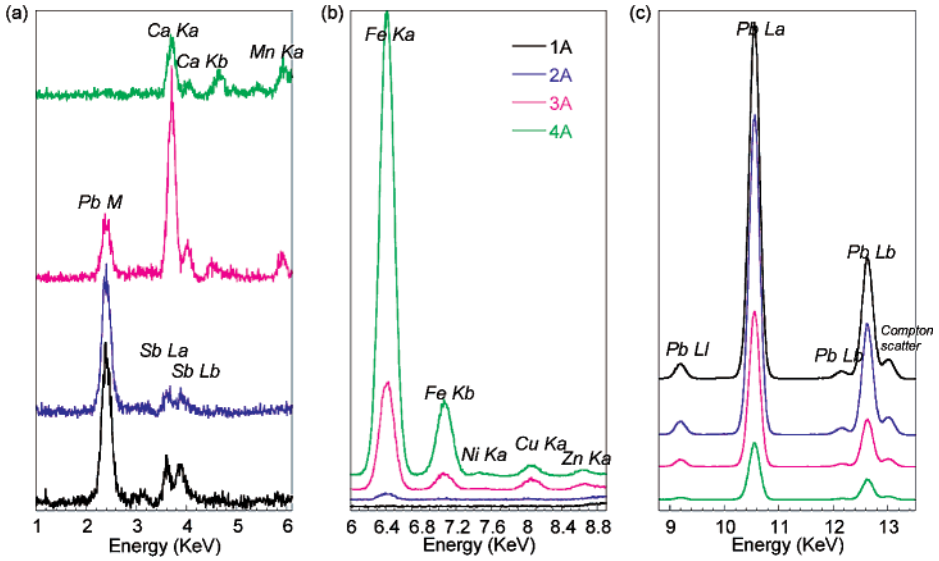

FIGURE 4. XRF spectra from sample A collected on NSLS beamline X26A. Spot locations are reported in Figure 2a. Spectra were collected with an incident beam of 13 035 eV.

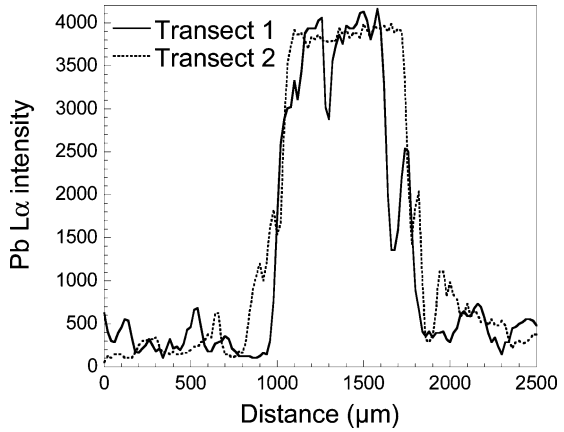

FIGURE 5. Pb concentration profile, according to the Pb Lα peak intensity of μ-XRF measurements, along transects 1 and 2 marked in Figure 2b.

micrometers distance from the crust material is also evident.

In addition to the fluorescence lines of Pb, lines at 3.605 keV (Sb $L\alpha_1$) and 3.844 keV (Sb $L\alpha_1$) are indicative of the relatively small amount of Sb in the bullet cores (2−4% by weight) (Figure 4a). Other metals were not detected by XRF in the bullet core. However, the weathering crust shows traces of Fe (Figure 4b, spot 2A), which may stem from the surrounding soil or from the corroded bullet jackets. This result is in agreement with the XRD observations and previous reports (*19*, *20*) showing that the crust is forming by oxidation of metallic Pb and Sb and incorporation of elements provided by the surrounding soil. The elements Fe, Cu, Zn, Ca, Ni, and Mn are also clearly detectable in spots 3A and 4A (Figure 4). However, in the soil surrounding the corroding bullets, the spatial distribution of Pb exhibits no positive correlation with the distributions of those elements.

Micro-X-ray Absorption Spectroscopy. To investigate the spatial variability of Pb species, we collected μ-XANES spectra at the Pb L_{III} edge. The μ-XANES spectra and corresponding first derivatives for the spots marked in Figures 3 and 4 are presented as dotted black lines in Figure 6, along with selected reference lead phases for comparison. The spectra are ranked according to relative Pb concentrations, with highest relative concentrations at spots 1A and 1B (bullet core) and lowest concentrations at spot 4A (soil matrix). For this purpose, the Pb concentration at each spot was qualitatively estimated from Pb Lα emission peak areas in μ-XRF spectra (Figure 4). Relative concentrations were then calculated with spot 1 as reference for the bullet core.

XANES near-edge features evolve from electron transitions from the core state to unoccupied valence states of the molecular cluster surrounding the X-ray absorbing atom (*30*). Hence small differences in the distortion, nature, and number of first neighbors around Pb give rise to substantial differences in the XANES spectra (*31*, *32*). While atoms beyond the coordination sphere may also contribute to the XANES spectra, their influence is much smaller as compared to the coordination sphere.

The electronic configuration of Pb is Xe $4f^{14}5d^{10}6s^26p^2$; thus, 6d is the first free electronic orbital. Hence, the Pb L_{III} edge corresponds to the electronic transition 2p → 6d. The edge position indicates the Pb valence, with the inflection point of metallic (zerovalent) Pb being assigned to 13 035 eV. A shift of +2 eV above this energy indicates, by comparison with standards, that divalent Pb prevails in the soil surrounding the bullets.

The XANES spectra and first derivatives of spots 1A and 1B (bullet cores) are identical to that of a metallic Pb foil (not shown). The XANES spectra and first derivatives collected on spots 2A and 2B were similar to the reference spectra for litharge. The edge position of 13 054 eV is in line with Pb(II). Further, a pre-edge feature is clearly visible at 13 029 eV. Bargar et al. (*31*), Eiden-Assmann et al. (*33*), and Rao and Wong (*32*) assigned it to the electronic transition 2p → 6s. If Pb is tetravalent, 6s is a free electronic orbital and this peak always occurs (*31*). When Pb is divalent, 6s is an occupied orbital. This transition can occur only if the 6s electronic orbital is hybridized, which is allowed in case of PbO where the $6s^2$ pairs are commonly described as stereochemically active (*34*). However, the nature of this hybridization remains uncertain. Several authors, on the basis of XANES and NMR experiments, have assigned it to Pb 6s−6p promotions, which can exist only in certain symmetries such as the C_{4v} square-pyramidal environment of Pb(II) in litharge (*31*, *33*, *35*). Other authors, on the basis of ab initio calculations in density functional theory (DFT), have assigned it to Pb 6s−O 2p hybridization (*36*, *37*). Recently, Farges et al. (*38*) showed by ab initio calculations with FEFF that this pre-peak could also

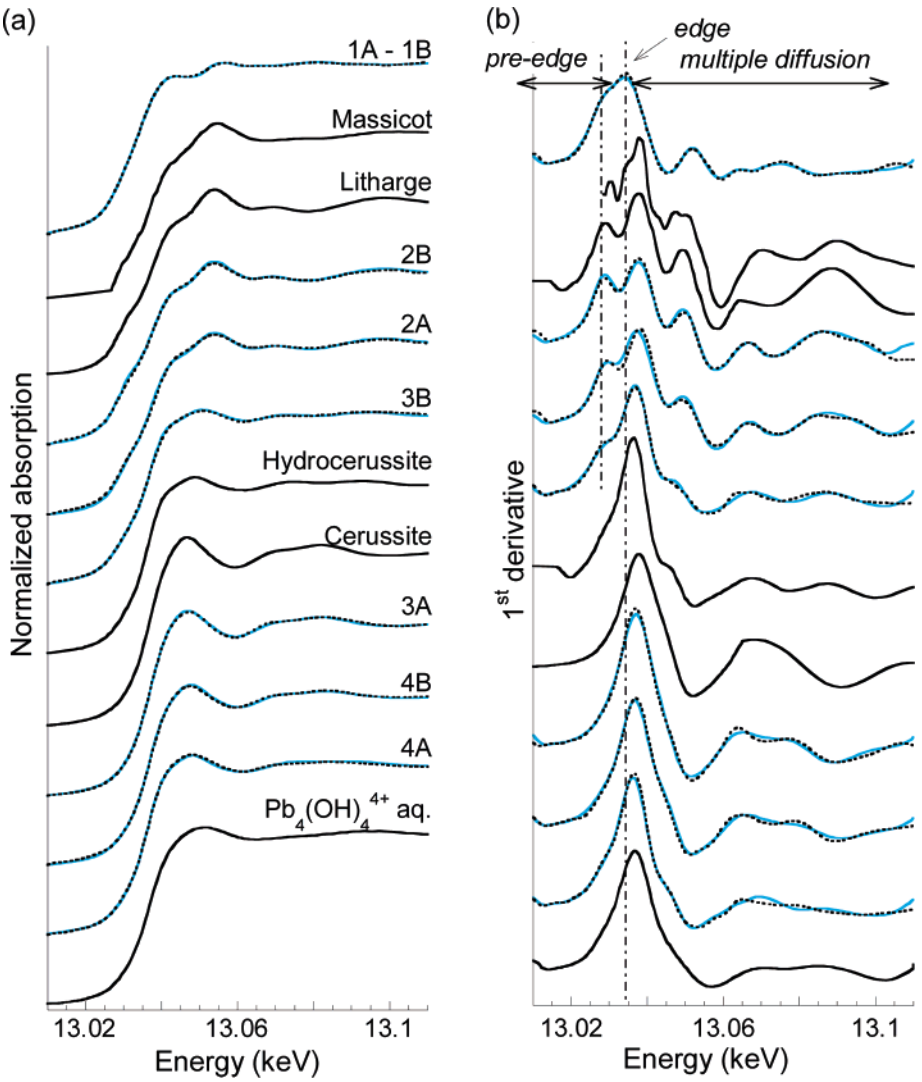

FIGURE 6. Normalized μ-XANES spectra (a) and corresponding first derivatives (b) of samples A and B (dotted lines), sorted along decreasing Pb concentration from top to bottom. The blue lines are the linear combination fits (Table 3) based on the reference spectra, which are shown as black solid lines. Spot locations are as in Figure 2a.

arise from multiple scattering of the photoelectron among neighboring atoms.

The spectra collected on spot 3B showed a weak pre-edge feature similar to that of litharge, but the edge features are more similar to those of hydrocerussite. Thus, both litharge and hydrocerussite may contribute to this spectrum. The spectra collected at spots 3A, 4B, and 4A also indicate mixtures of hydrocerussite, cerussite, and possibly aqueous or adsorbed Pb^{2+}. Note, that the reference spectrum for $Pb_4(OH)_4^{4+}$-(aq) was chosen, because this species has a distorted trigonal pyramidal coordination, which is similar to inner-sphere sorption complexes of Pb on surfaces (*39*).

Linear Combination Fitting. The XANES spectra suggest that several lead compounds may coexist in the different areas surrounding the corroding bullets. To assess their nature and quantity, we performed linear combinations fits using reference spectra. The curves representing the best-fit linear combinations are plotted as blue lines in Figure 6. The corresponding fitting parameters are reported in Table 3. The set of reference compounds used for linear combination fitting represents the most likely lead species in soils (*29*). Relative concentrations derived by the linear least-squares fitting approach should, in general, be considered accurate to ±25% of their stated value. Contributions of less than 10% should be viewed with caution (*40*). Thus, for the final fit, we kept as few components as possible and removed components with little abundance since they did not significantly improve the fitting result. The fits are considered valid since the least-squares fit residual values (χ^2) are less than 200 (except for two samples where they are around 700), residuals are below 0.95, and the sum of components ranged from 98.42% to 100.3%.

TABLE 3. Abundance of Reference Pb Species in Experimental μ-XANES Spectra[a]

spot	[Pb]/[Pb]$_{bullet}$	Pb(0)	L	H	C	$Pb_4(OH)_4^{4+}$	sum (%)	residual (%)	χ^2
1B	1	100					100.9	1.19	226.86
1A	1	100					101.1	0.86	148.11
2B	0.99		85	15			98.3	0.70	54.98
2A	0.98		70	30			100.1	0.95	139.05
3B	0.96		45	30	25		98.3	0.94	168.50
3A	0.83			20	80		99.7	0.61	64.53
4B	0.65			40	60		97.1	0.77	51.10
4A	0.58			20	30	50	99.6	0.99	239.23

[a] Abundance is calculated by linear combination fitting and sorted according to Pb content. Pb(0) = metallic Pb, L = litharge, H = hydrocerussite, C = cerussite. Sum (%) is the real sum of given reference spectra partial concentrations. Residual (%) and χ^2 are deviations resulting from the least-squares refinement.

Discussion of the Weathering Process. The results support the successive formation of litharge, hydrocerussite, cerussite, and cationic Pb^{2+}, in agreement with thermodynamic data (*29*). Oxides of Pb (PbO and PbO_2) are potentially the first products resulting from the direct oxidation of metallic lead by oxygen. Since formation of PbO_2 is unlikely at the prevalent redox conditions in soils, only PbO occurs ($Pb + {}^1/_2O_2 \rightarrow PbO$). In previous studies, massicot (β-PbO) was reported as the PbO phase formed in bullet corrosion (*15*, *20*−*22*) and litharge (α-PbO) as the PbO phase formed in corroded artifacts and antic lead pipes (*23*, *24*). In our study, linear combination fits performed with massicot as reference were not satisfactory. XANES spectra of litharge and massicot have similar shapes (*41*), but the spectral features are more pronounced in the litharge spectrum. The latter exhibits a single peak at 13 071 eV, which was also observed in the spectra of spots 2A and 2B but does not exist in the massicot spectrum. Thus litharge is the PbO phase present in this studied soil. Although at atmospheric pressure and temperature tetragonal α-PbO (litharge) is predicted to predominate (*36*, *42*, *43*), both massicot and litharge were observed in natural systems. Possibly, there is an influence of the sample pretreatment and detection method. Massicot was evidenced in studies where corrosion products were collected by use of an ultrasonic bath or when fast weathering in the laboratory was performed. Litharge was detected in studies performing in situ analysis of nonpretreated samples, as in our study. Massicot may be a metastable, fast-forming PbO phase that converts into litharge with time (*23*).

Lead oxide is the most soluble mineral of those considered here. It can be easily converted to other compounds such as $Pb(OH)_2$, $PbSO_4$, $PbCO_3$, and $Pb_3(CO_3)_2(OH)_2$ (*29*). Due to the low abundance of sulfur in the soil (450 mg kg^{-1}), the formation of anglesite [$PbSO_4$] is not favored. At CO_2 partial pressures $P_{CO2} \geq 0.0003$ atm and 25 °C, the formation of cerussite is thermodynamically favored over the formation of hydrocerussite (*23*, *29*). However, according to our results (Table 3) and in agreement with Lin (*15*), hydrocerussite is the first carbonated species formed in the weathering crust. The competitive equilibrium reactions are (*29*)

$$\alpha\text{-PbO(c)} + 2H^+ \rightleftharpoons Pb^{2+} + H_2O \quad (\log K = 12.72) \tag{1}$$

$$Pb_3(CO_3)_2(OH)_2(c) + 6H^+ \rightleftharpoons 3Pb^{2+} + 2CO_2(g) + 4H_2O \quad (\log K = 17.51) \tag{2}$$

$$PbCO_3(c) + 2H^+ \rightleftharpoons Pb^{2+} + CO_2(g) + H_2O \quad (\log K = 4.65) \tag{3}$$

By combining eqs 2 and 3 to yield eq 4, one can predict that hydrocerussite is favored when the ratio of water activity to P_{CO2} is larger than $10^{3.56}$, which may be the case at the interface between the metallic Pb core and the weathering crust of the bullets. If the activity of water is unity, this corresponds to a CO_2 partial pressure of $P_{CO2} = 0.000\,275$ atm. With increasing P_{CO2} toward the outer surface of the weathering crust, hydrocerussite is then transformed into cerussite following the reaction

$$Pb_3(CO_3)_2(OH)_2(s) + CO_2(g) \rightleftharpoons 3PbCO_3(s) + H_2O \quad (\log K = 3.56) \tag{4}$$

The dissolution of cerussite controls the activity of Pb^{2+} in the soil solution in contact with the corroding lead bullets. At atmospheric partial pressure of CO_2 ($P_{CO2} = 0.000\,35$ atm) and pH 7, the activity of Pb^{2+} in solution in equilibrium with cerussite at 25 °C is 1.28×10^{-6}. Due to soil respiration, the CO_2 partial pressure in soils is usually strongly elevated and can exceed 0.02 atm even in well-aerated soils. Since the solubility of cerussite decreases proportionally with increasing P_{CO2}, the activity of Pb^{2+} in the soil solution in contact with the corroding Pb bullets is expected to be even lower. Dissolved Pb^{2+} diffusing away from the weathering crust into the soil matrix is strongly adsorbed to minerals and soil organic matter, resulting in low mobility of Pb in the soil.

In summary, we have shown that the spatial distribution and speciation of Pb in the weathering crust of Pb bullets in soils can be studied by μ-XRF elemental mapping and synchrotron μ-XANES spectroscopy. In contrast to previous studies, we found litharge (α-PbO) to be the first weathering product occurring near the metallic Pb core. In the presence of CO_2, litharge is transformed to hydrocerussite [$Pb_3(CO_3)_2(OH)_2$] and then to cerussite ($PbCO_3$), which was the dominating Pb phase in the weathering crust of the corroding bullets.

Acknowledgments

We thank Michael Plötze (ETH Zurich) for powder XRD analysis, Kurt Barmettler and Irene Xifra (ETH Zurich) for their support with soil analyses, and Bill Rao (Consortium for Advanced Radiation Sources, University of Chicago) for his help with μ-XANES measurements at NSLS beamline X26. Research carried out at the National Synchrotron Light Source, Brookhaven National Laboratory, was supported by the U.S. Department of Energy, Division of Materials Sciences, under Contract DE-AC02-98CH10886. Use of the Beamline X26A was supported by the Department of Energy, Basic Energy Science's Geosciences Research Program under Grant DE-FG02-92ER14244.

Literature Cited

(1) Adriano, D. C. *Trace Elements in Terrestrial Environments: Biogeochemistry, Bioavailability, and Risks of Metals*; Springer: New York, 2001.

(2) Rice, D. A.; McLoughlin, M. F.; Blanchflower, W. J.; Thompson, T. R. Chronic lead-poisoning in steers eating silage contaminated with lead shot diagnostic-criteria. *Bull. Environ. Contam. Toxicol.* **1987**, *39*, 622−629.

(3) Wixson, B. G.; Davies, B. E. Guidelines for lead in soil—proposal of the Society for Environmental Geochemistry and Health. *Environ. Sci. Technol.* **1994**, *28*, A26−A31.

(4) Rooney, C. P.; McLaren, R. G.; Cresswell, R. J. Distribution and phytoavailability of lead in a soil contaminated with lead shot. *Water Air Soil Pollut.* **1999**, *116*, 535−548.

(5) Lewis, L. A.; Poppenga, R. J.; Davidson, W. R.; Fischer, J. R.; Morgan, K. A. Lead toxicosis and trace element levels in wild birds and mammals at a firearms training facility. *Arch. Environ. Contam. Toxicol.* **2001**, *41*, 208−214.

(6) Mozafar, A.; Ruh, R.; Klingel, P.; Gamper, H.; Egli, S.; Frossard, E. Effect of heavy metal contaminated shooting range soils on mycorrhizal colonization of roots and metal uptake by leek. *Environ. Monit. Assess.* **2002**, *79*, 177−191.

(7) Davies, B. E. Lead. In *Heavy Metals in Soils*; Alloway, B. J., Ed.; Blackie Academic & Professional: London, 1995; pp 206−223.

(8) Manceau, A.; Boisset, M. C.; Sarret, G.; Hazemann, R. L.; Mench, M.; Cambier, P.; Prost, R. Direct determination of lead speciation in contaminated soils by EXAFS spectroscopy. *Environ. Sci. Technol.* **1996**, *30*, 1540−1552.

(9) Jorgensen, S. S.; Willems, M. The fate of lead in soils—the transformation of lead pellets in shooting-range soils. *Ambio* **1987**, *16*, 11−15.

(10) Mellor, A.; McCartney, C. The effects of lead shot deposition on soils and crops at a clay pigeon shooting site in northern England. *Soil Use Manage.* **1994**, *10*, 124−129.

(11) Scheuhammer, A. M.; Norris, S. L. The ecotoxicology of lead shot and lead fishing weights. *Ecotoxicology* **1996**, *5*, 279−295.

(12) BUWAL. Wegleitung: Bodenschutz- und Entsorgungsmassnahmen bei 300m Schiessanlagen. Generalsekretariat EMD, Bundesamt für Umwelt, Wald und Landschaft (BUWAL), Bern, Switzerland, 1997.

(13) Fahrenhorst, C.; Renger, M. Auswirkungen sehr hoher Gehalte an Blei, Antimon und Arsen bei landwirtschaftlich genutzten Böden im Immissionsbereich von Schiessplätzen. *VDLUFA Kongressber.* **1990**, *32*, 827−830.

(14) Manninen, S.; Tanskanen, N. Transfer of lead from shotgun pellets to humus and 3 plant-species in a Finnish shooting range. *Arch. Environ. Contam. Toxicol.* **1993**, *24*, 410−414.
(15) Lin, Z. X. Secondary mineral phases of metallic lead in soils of shooting ranges from Orebro County, Sweden. *Environ. Geol.* **1996**, *27*, 370−375.
(16) Basunia, S.; Landsberger, S. Contents and leachability of heavy metals (Pb, Cu, Sb, Zn, As) in soil at the Pantex firing range, Amarillo, Texas. *Air Waste Manage. Assoc.* **2001**, *51*, 1428−1435.
(17) Knechtenhofer, L.; Xifra, I.; Scheinost, A. C.; Flühler, H.; Kretzschmar, R. Fate of heavy metals in a strongly acidic shooting-range soil: Small-scale metal distribution and its relation to preferential water flow. *J. Plant Nutr. Soil Sci.* **2003**, *166*, 84−92.
(18) Sénat. Effets des métaux lourds sur l'environnement et la santé, Sénat, 2002.
(19) Lin, Z. X.; Comet, B.; Qvarfort, U.; Herbert, R. The chemical and mineralogical behavior of Pb in shooting range soils from central Sweden. *Environ. Pollut.* **1995**, *89*, 303−309.
(20) Chen, M.; Daroub, S. H.; Ma, L. Q.; Harris, W. G.; Cao, X. D. Characterization of lead in soils of a rifle/pistol shooting range in central Florida, USA. *Soil Sediment. Contam.* **2002**, *11*, 1−17.
(21) Cao, X. D.; Ma, L. Q.; Chen, M.; Hardison, D. W.; Harris, W. G. Weathering of lead bullets and their environmental effects at outdoor shooting ranges. *J. Environ. Qual.* **2003**, *32*, 526−534.
(22) Hardison, D. W.; Ma, L. Q.; Luongo, T.; Harris, W. G. Lead contamination in shooting range soils from abrasion of lead bullets and subsequent weathering. *Sci. Total Environ.* **2004**, *328*, 175−183.
(23) Essington, M. E.; Foss, J. E.; Roh, Y. The soil mineralogy of lead at Horace's villa. *Soil Sci. Soc. Am. J.* **2004**, *68*, 979−993.
(24) Reich, S.; Leitus, G.; Shalev, S. Measurement of corrosion content of archeological lead artifacts by their Meissner response in the superconducting state, a new dating method. *New J. Phys.* **2003**, *5*, 991−999.
(25) Thomas, G. W. Soil pH and soil acidity. In *Methods of Soil Analysis. Part 3—Chemical Methods*; Sparks, D. L., Ed.; *Soil Sci. Soc. Am. Book Ser.* **1996**, *3*.
(26) Zeien, H.; Brümmer, G. W. Chemische Extraktionen zur Bestimmung von Schwermetallbindungsformen in Böden. *Mitt. Dtsch. Bodenkd. Gesellsch.* **1989**, *59*, 505−510.
(27) Lanzirotti, A.; Miller, L. M. Imaging and microspectroscopy at the national synchrotron light source. *Synchrotron Radiat. News* **2002**, *15*, 17−26.
(28) Ressler, T. WinXAS: A program for X-ray absorption spectroscopy data analysis under MS-Windows. *J. Synchrotron Radiat.* **1998**, *5*, 118−122.
(29) Lindsay, W. L. *Chemical Equilibria in Soils*; John Wiley and Sons: New York, 1979.
(30) Brown, G. E., Jr.; Calas, G.; Waychunas, G. A.; Petiau, J. X-ray absorption spectroscopy: Applications in mineralogy and geochemistry. In *Spectroscopic Methods in Mineralogy and Geology*; Hawthorne, F. C., Ed.; *Rev. Mineral.* **1988**, *18*, 431−512.
(31) Bargar, J. R.; Brown, G. E., Jr.; Parks, G. A. Surface complexation of Pb(II) at oxide−water interfaces. 1. XAFS and bond-valence determination of mononuclear and polynuclear Pb(II) sorption products on aluminum oxides. *Geochim. Cosmochim. Acta* **1997**, *61*, 2617−2637.
(32) Rao, K. J.; Wong, J. A XANES investigation of the bonding of divalent lead in solids. *J. Chem. Phys.* **1984**, *81*, 4832−4843.
(33) Eiden-Assmann, S.; Schneider, A. M.; Behrens, P.; Wiebcke, M.; Engelhardt, G.; Felsche, J. Lead hydro sodalite $[Pb_2(OH)(H_2O)_3]_2$-$[Al_3Si_3O_{12}]_2$: Synthesis and structure determination by combining X-ray Rietveld refinement, ^{1}H MAS NMR FTIR and XANES spectroscopy. *Chem.-Eur. J.* **2000**, *6*, 292−297.
(34) Gabuda, S. P.; Kozlova, S. G. Relativistic effects in chemical interactions: Symmetry and polymorphism of inorganic heavy-metal compounds. *Russ. J. Inorg. Chem.* **2001**, *46*, S106−S128.
(35) Dybowski, C.; Gabuda, S. P.; Kozlova, S. G.; Neue, G.; Perry, D. L.; Terskikh, V. V. Correlation and relativistic effects in beta-PbO and other lead(II) oxides: A quantum ab initio explanation of ^{207}Pb NMR and XANES spectra. *J. Solid State Chem.* **2001**, *157*, 220−224.
(36) Terpstra, H. J.; Degroot, R. A.; Haas, C. Electronic structure of the lead monoxides—Band-structure calculations and photo-electron-spectra. *Phys. Rev. B* **1995**, *52*, 11690−11697.
(37) Watson, G. W.; Parker, S. C.; Kresse, G. Ab initio calculation of the origin of the distortion of alpha-PbO. *Phys. Rev. B* **1999**, *59*, 8481−8486.
(38) Farges, F.; Brown, G. E., Jr.; Rehr, J. J. Ti K-edge XANES studies of Ti coordination and disorder in oxide compounds: Comparison between theory and experiment. *Phys. Rev. B* **1997**, *56*, 1809−1819.
(39) Astrup, T.; Boddum, J. K.; T. H., C. Lead distribution and mobility in a soil embankment used as a bullet stop at a shooting range. *J. Soil Contam.* **1999**, *8*, 653−665.
(40) Ostergren, J. D.; Brown, G. E., Jr.; Parks, G. A.; Tingle, T. N. Quantitative speciation of lead in selected mine tailings from Leadville, CO. *Environ. Sci. Technol.* **1999**, *33*, 1627−1636.
(41) Yu, Y. H.; Tyliszczak, T.; Hitchcock, A. P. Pb L_3 EXAFS and near-edge studies of lead metal and lead oxides. *J. Phys. Chem. Solids* **1990**, *51*, 445−451.
(42) Haussermann, U.; Berastegui, P.; Carlson, S.; Haines, J.; Léger, J. M. TlF and PbO under high pressure: unexpected persistence of the stereochemically active electron pair. *Angew. Chem., Int. Ed.* **2001**, *40*, 4624−4629.
(43) Adams, D. M.; Christy, A. G.; Haines, J.; Clark, S. M. Second-order phase transition in PbO and SnO at high pressure: Implications for the litharge-massicot phase transformation. *Phys. Rev. B* **1992**, *46*, 11358−11367.

Received for review November 5, 2004. Revised manuscript received March 25, 2005. Accepted April 11, 2005.

ES0482740